Available online at www.sciencedirect.com
ScienceDirect
Journal of Constructional Steel Research 63 (2007) 1036–1050
JOURNAL OF CONSTRUCTIONAL STEEL RESEARCH
www.elsevier.com/locate/jcsr

Strength design criteria for steel members at elevated temperatures

Jiro Takagi*, Gregory G. Deierlein

John A. Blume Earthquake Engineering Center, Department of Civil and Environmental Engrg. - MC 4020, Stanford University, Stanford, CA 94305-4020, United States

Received 3 August 2006; accepted 23 October 2006

Abstract

Design equations for structural steel members at elevated (fire) temperatures are evaluated through comparisons with nonlinear finite element simulations. The study includes comparative analyses of the American Institute of Steel Construction (AISC) and European Committee for Standardization (CEN) design provisions for laterally unsupported I-shaped columns, beams, and beam–columns at temperatures between ambient to 800 °C. The Eurocode 3 provisions are shown to predict the simulated finite element results within about 10%–20%. On the other hand, the AISC specification predicts strengths that are up to twice as large (unconservative) as the simulated results. The discrepancies are largest for members of intermediate slenderness and temperatures above 300 °C. Modifications to the AISC equations are proposed that provide improved accuracy with calculated strengths typically within 20%–30% of the simulated results. Limitations of the member-based assessments and future research and development needs for structural fire engineering are discussed.

Keywords: Fire; Elevated temperatures; Stability; Steel members; Design equations

1. Introduction

While the basic concepts for structural fire engineering are well established, explicit assessment of structural response to fires is uncommon in engineering practice. Instead, building codes and design practice have traditionally relied on prescriptive requirements to provide adequate structural fire-resistance in building structures. In steel-framed structures, this is typically accomplished through thermal insulation requirements that are validated by fire endurance tests. Such approaches may work well for routine design, however, the lack of alternative methods to establish structural performance by calculation impedes the design of structures where the prescriptive methods fall short of providing effective solutions. Recently, the situation is changing with the publication of standards to calculate structural fire resistance in a manner similar to how other strength limit states are evaluated. For example, the Eurocode 3 (EC3) standard [1] includes detailed provisions to establish fire loads and evaluate their effects on steel structures. The latest edition of the *Specification for Structural Steel Buildings* in the American Institute of Steel Construction (AISC) [2] includes a new appendix entitled, *Structural Design for Fire Conditions*, which provides guidance and criteria to evaluate the structural resistance of steel building components at elevated temperatures.

The EC3 and AISC standards for steel structures both follow an approach whereby the structural resistance to gravity and other loads is calculated with the steel members at an assumed elevated temperature. Each standard permits this evaluation through either an "advanced" or "simple" method, where the former requires rigorous structural and thermal simulations and the latter method is accomplished through member-based strength limit state checks. The member-based approaches are similar to conventional checks made at ambient temperatures. In the AISC specification, for example, the member design strength equations are essentially the same as those for ambient temperatures, except that the input yield strength and elastic modulus of the steel are reduced based on the assumed elevated temperature. While the AISC method is straightforward and easy to implement, its accuracy has not been thoroughly verified. On the other hand, the structural fire provisions of EC3 have been published in codified form since the early 1990's and have been reviewed and modified since their first publication.

* Corresponding author. Tel.: +1 650 725 3168; fax: +1 650 725 9755.
E-mail addresses: jtakagi@stanford.edu (J. Takagi), ggd@stanford.edu (G.G. Deierlein).

0143-974X/$ - see front matter © 2006 Elsevier Ltd. All rights reserved.
doi:10.1016/j.jcsr.2006.10.005

Symbols

A	Cross-sectional area
C_w	Warping constant
C_X	Exponent in equation for proposed critical moment
E	Modulus of elasticity
F_e	Elastic buckling stress
F_L	Initial yield stress
F_p	Stress at the proportional limit
F_r	Residual stress
F_y	Yield stress
G	Shear modulus of elasticity
I_x, I_y	Moment of inertia about strong and weak axis
J	Torsional constant
K	Effective buckling length factor
K_p, K_y, K_E	Reduction factors for the proportional limit, yield stress, and modulus of elasticity respectively
L	Length
M_p	Plastic moment
M_r	Initial yield moment
$M_{\mathrm{cr,AISC}}$, ($M_{\mathrm{cr}x,\mathrm{AISC}}$)	Nominal moment (about strong axis) in AISC
$M_{\mathrm{cr,EC3}}$, ($M_{\mathrm{cr}x,\mathrm{EC3}}$)	Nominal moment (about strong axis) in EC3
$M_{\mathrm{cr,Prop}}$, ($M_{\mathrm{cr}x,\mathrm{Prop}}$)	Proposed nominal moment (about strong axis)
$M_{\mathrm{cr},e}$	Elastic critical moment
M_{ux}	Factored bending moment about strong axis
$M_{x,\mathrm{end}}$	Bending moment about strong axis at the ends
$P_{\mathrm{cr,AISC}}$, ($P_{\mathrm{cr}y,\mathrm{AISC}}$)	Nominal axial strength of column (for flexural buckling about weak axis) in AISC
$P_{\mathrm{cr,EC3}}$, ($P_{\mathrm{cr}y,\mathrm{EC3}}$)	Nominal axial strength of columns (for flexural buckling about weak axis) in EC3
$P_{\mathrm{cr,Prop}}$, ($P_{\mathrm{cr}y,\mathrm{Prop}}$)	Proposed nominal axial strength of column (for flexural buckling about weak axis)
P_u	Factored axial load
S_x	Elastic section modulus about strong axis
Z_x	Plastic section modulus about strong axis
T	Temperature
b_f	Flange width of section
h	Height of section
r	Governing radius of gyration
r_x, r_y	Radius of gyration about strong and weak axis
t_f, t_w	Flange and web thickness of section. respectively
α	Imperfection factor for flexural buckling in EC3
α_{LT}	Imperfection factor for lateral–torsional buckling in EC3
α_x, α_y	Imperfection factor for flexural buckling about strong and weak axis in EC3
λ	Slenderness ratio in AISC
$\overline{\lambda}$	Slenderness ratio for flexural buckling in EC3
$\overline{\lambda}_{LT}$	Slenderness ratio for lateral torsional buckling in EC3
λ_p	Slenderness ratio for transition between full plastic bending and inelastic lateral–torsional buckling in AISC
λ_r	Slenderness ratio for transition between inelastic and elastic lateral–torsional buckling in AISC
λ_{rf}, λ_{rw}	Limiting width–thickness ratio for local buckling of flange and web in AISC
χ	Reduction factor for flexural buckling in EC3
χ_{LT}	Reduction factor for lateral torsional buckling in EC3

The objective of this study is to provide a critical assessment of the AISC and EC3 member strength equations through a comparison with results of detailed finite element simulations at elevated temperatures. The assessment includes laterally unsupported columns, beams, and beam–columns of bi-symmetric I-shaped steel sections with idealized loading and boundary conditions. The simulations employ three dimensional shell finite element models that capture inelastic yielding, overall and local buckling, and non-uniform torsion effects. The column strengths are evaluated in terms of critical axial loads applied to pin-ended columns with initial geometric imperfections that represent fabrication tolerances. The beam strengths are evaluated in terms of critical bending moments, which are applied about the major-axis at the ends of a simply supported beam that is laterally unsupported and susceptible to lateral–torsional buckling. The results are then compared for the combined effects of axial compression and bending in beam–columns. The assessment covers a range of design conditions by parametrically varying the elevated temperatures and member lengths. Most of the analyses are for members of Grade 50 steel (yield strength of $F_y = 345$ MPa) with selected study of Grade 36 ($F_y = 250$ MPa) steel.

As will be demonstrated, the AISC strength equations at elevated temperatures are unconservative, and alternative strength equations are proposed. The proposed equations are similar in format to the AISC provisions, thus maintaining practicality for design. Beyond the immediate benefit of the improved design equations, this research provides fundamental information to improve the understanding of structural steel members under fire conditions.

2. Basis of member strength evaluations

Assessment of structural safety to fire hazards can generally be categorized into three stages. The first stage entails characterization of fire initiation and development, which can be done either through direct simulation or through parametric time–temperature models of compartment gas temperatures. The second stage involves heat transfer calculations to evaluate temperatures in structural members, considering insulation and other factors that affect heat transfer. The third stage is to assess structural behavior under elevated temperatures, including the effects of both thermal expansion and degradation of material properties. The assessments made within each of these three stages are generally treated as conditionally

independent, where it is assumed that structural behavior does not impact heat transfer or fire development and heat transfer does not impact fire development. While there are situations where the assumption of conditional independence does not hold (e.g., where structural deformations may damage fire compartments, which in turn affects fire development), in most cases the conditional independence is a reasonable assumption. This assumption greatly simplifies the assessment since the analyses in each stage can be done separately and without interaction. This line of reasoning is implicit in the structural fire assessment presented herein (and in the AISC and EC3 design provisions), where the elevated steel temperatures are treated as input to the structural assessment and calculated independently.

In this study, it is assumed that the elevated temperature of the steel members is known (or can be determined) and used to evaluate the strength limit state of individual members under the combined effects of elevated temperature and applied loads. In concept, the strength limit state can then be evaluated either by (1) calculating the critical temperature (intensity and distribution) that the member can sustain under the given loads, or (2) calculating the strength (load resistance) of a member under a specified temperature. The former approach, referred to herein as the "temperature approach", is more representative of the actual fire conditions, where the temperature increases while the applied gravity loads are constant. The latter approach (termed the "load approach") is simpler to implement in nonlinear analysis and fits more naturally in existing formats for structural assessment, where member design equations or simulation tools (e.g., nonlinear analysis) are used to assess the critical loads based on the specified temperature-dependent material properties. Although material nonlinear analyses are, in concept, load path dependent, for monotonically increasing gravity loads and temperatures of individual members, it is reasonable to assume that the critical limit state calculated following a "temperature approach" and "load approach" should be similar. The authors have confirmed this assumption by conducting finite element analyses of individual members with fixed loads and variable temperature and vice versa. Shown in Fig. 1 is an example of one such analysis, where the critical combinations of temperature and strength for a column are obtained by both approaches. This example is for a W14 × 90 Grade 50 column (W360 × 134; $F_y = 345$ MPa) with a length of 5.67 m and weak axis slenderness ratio of 60. The column was modeled using shell finite elements, where its strength limit state is controlled by flexural buckling about the weak axis. Further details of finite element analyses are described later.

The AISC design provisions essentially adopt the load approach concept, where the member resistance under a specified temperature is obtained by substituting a degraded modulus of elasticity and yield stress into strength design equations that are otherwise the same as those applied at ambient temperatures. This member-based check further assumes that the loads induced in the member by restraint to thermal expansion can be independently calculated and superimposed with other applied load effects. The extent to

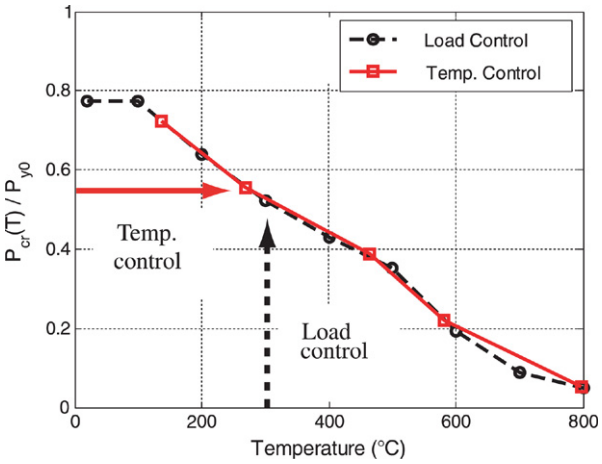

Fig. 1. Comparison of temperature and load control analyses.

which this assumption is valid depends on the indeterminate nature of the structural system and loading — effects that are not represented in an isolated member analysis. Another assumption made in the AISC provisions and this study is that the member strength can be conservatively calculated with a uniform temperature distribution through the member.

2.1. Steel properties under elevated temperatures

Shown in Fig. 2(a) are idealized stress–strain curves for steel at elevated temperatures. These curves are based on parameters specified in EC3 and substantiated by test data collected by Wainman and Kirby [3] and others. These stress–strain models are specified through reduction factors (see Fig. 2(b)–(c)), which are defined for the proportional limit F_p, yield stress F_y, and modulus of elasticity E as follows:

$$K_p(T) = \frac{F_p(T)}{F_{p0}}, \qquad K_y(T) = \frac{F_y(T)}{F_{y0}}$$

$$\text{and} \qquad K_E(T) = \frac{E(T)}{E_0}. \tag{1}$$

The terms in the denominator of Eq. (1), F_{p0}, F_{y0}, and E_0, correspond to properties at ambient temperature (20 °C), and those in the numerator, $F_p(T)$, $F_y(T)$, and $E(T)$, are at the elevated temperature, T. Values of the reduction factors are summarized in Table 1 and plotted in Fig. 2(c). Referring to Fig. 2(c), at 600 °C the yield strength decreases to about half its ambient temperature value, while the elastic modulus and proportional limit decrease more rapidly to about 30% and 20%, respectively, of their ambient values.

Referring back to Fig. 2(a), the bilinear elastic plastic relationship, which is commonly assumed in idealized stress–strain models at ambient temperature, disappears as the material becomes more inelastic under elevated temperatures. Finite element analyses that employ nonlinear stress–strain curves (such as in Fig. 2(a)) model directly this behavior. As described later, the EC3 member design equations for elevated temperatures take this nonlinear stress–strain response into account through coefficients that vary nonlinearly with temperature. On the other hand, the AISC design equations

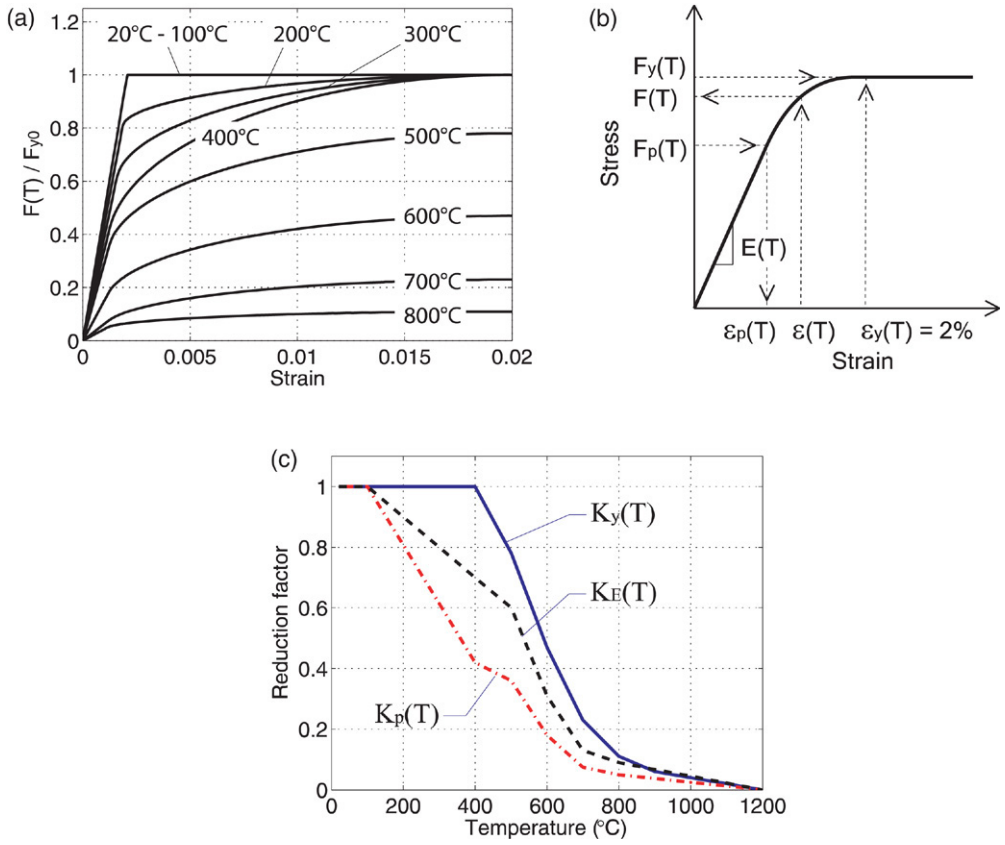

Fig. 2. Stress–strain response at high temperatures as defined by EC3, (a) stress–strain curves, (b) key parameters of the stress–strain curve, (c) reduction factors.

Table 1
Stress–strain reduction factors in EC3

Temperature (°C)	$K_y(T)$	$K_p(T)$	$K_E(T)$
20	1.000	1.000	1.000
100	1.000	1.000	1.000
200	1.000	0.807	0.900
300	1.000	0.613	0.800
400	1.000	0.420	0.700
500	0.780	0.360	0.600
600	0.470	0.180	0.310
700	0.230	0.075	0.130
800	0.110	0.050	0.090
900	0.060	0.038	0.068
1000	0.040	0.025	0.045
1100	0.020	0.013	0.023
1200	0	0	0

only apply reduction factors to the modulus of elasticity and the yield stress, thereby implying that the bilinear (elastic–plastic) properties are preserved at high temperatures. As described later, this assumption of bilinear behavior, which fails to take into account the graduate softening response, leads to unconservative results using the AISC member strength equations for elevated temperatures.

3. Finite element simulation model

Accuracy of the design models is judged against simulation data of detailed three-dimensional analyses of beam–columns

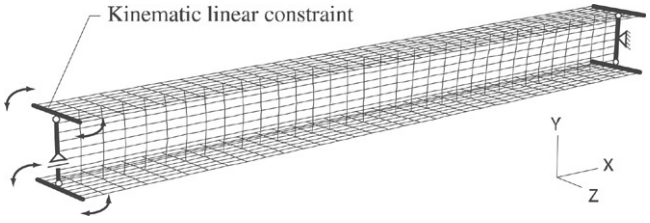

Fig. 3. Shell finite element mesh and boundary conditions.

using the finite element method (FEM). As shown in Fig. 3, the steel members are simulated with shell finite element models created and run using the ABAQUS software [4]. The shell finite element models are well suited to simulating geometric and material nonlinearity, including global flexural and torsional–flexural buckling and local flange and web buckling. The analyses are conducted using the "load approach" where the critical strength is determined by incrementing the applied load on a model at various prescribed temperatures. The following are some features of the models:

1. The member is subdivided into 32 shell elements along its length, and the flanges and web are each subdivided into eight elements across the cross section (Fig. 3). Each element has eight nodes and four Gaussian integration points in the shell plane with three point Simpson's rule integration through the shell thickness.
2. Nonlinear stress–strain curves of steel at the elevated temperatures are adopted from EC3, as shown in Fig. 2(a).

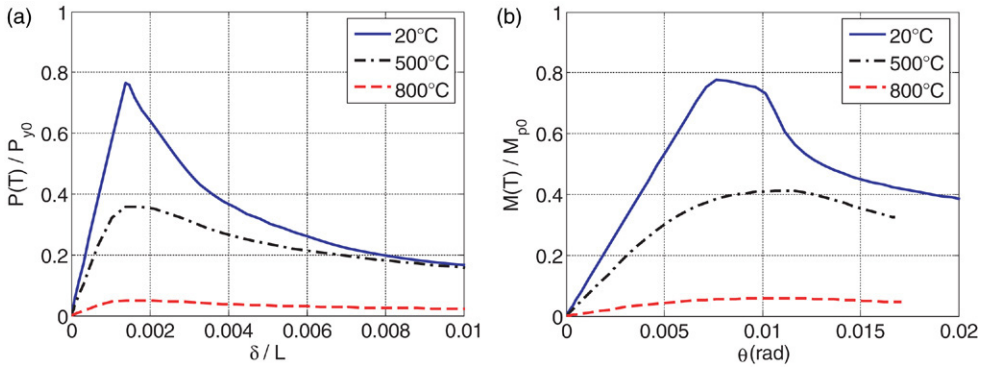

Fig. 4. Load versus displacement response from FEM simulations under ambient and elevated temperatures (a) W14 × 90 column ($L/ry = 60$ Gr. 50), (b) W14 × 22 beam ($L/ry = 60$, Gr. 50).

A uniform temperature distribution is assumed through the member cross section and along its length. Multiaxial yielding is modeled through the von-Mises yield criterion. The yield strengths are assumed to be equal to their nominal specified values, so as to provide consistent comparisons with the design models.

3. Linear kinematic constraints are applied to the flanges and web at the member end so as to enforce planar behavior within each flange and web but to allow cross-section warping (Fig. 3). Displacements of the web along the Y- and Z-axis are restrained at both ends and longitudinal displacements along the X-axis are restrained at one end. Twisting rotation (about the X-axis) is restrained at both ends, and rotational displacements about Y- and Z-axes (weak and strong axes) are free at both ends.
4. For the column (axial) strength analyses, axial forces are applied along the kinematically restrained webs and flanges at one end of the member. In one set of analyses, the flange ends are free to rotate, thereby permitting flexural buckling about the Y-axis (weak axis); and in a second set of analyses, rotational displacements about the Y-axis are restrained in order to determine the flexural buckling strength about the Z-axis (strong axis).
5. For the beam (flexural) strength analyses, a concentrated force couple is applied at the center of the upper and lower flanges at each end so as to induce a uniform strong axis moment along the beams. The kinematic constraint across the flanges ensures a uniform distribution of flexural stresses.
6. Initial geometric member "sweep" imperfections are modeled by introducing a single sinusoidal curve along the member length, with a maximum initial displacement of 1/1000 of the length at the mid-span.

Shown in Fig. 4 are example FEM simulation results for a laterally unsupported column and beam at ambient and elevated temperatures (20, 500, and 800 °C). Column results (Fig. 4(a)) are shown in terms of the normalized axial load versus midspan deflection for a W14 × 90 column with a slenderness of $L/r_y = 60$, where L is the length and r_y is radius of gyration about weak axis. The critical strength at 500 °C is about 50% of that at room temperature. This 50% reduction is in contrast to the three material reduction factors of K_y (500 °C) = 0.78, K_p (500 °C) = 0.36 and K_E (500 °C) = 0.60, whose range of values suggests that all three parameters, including the change in proportional limit, play a role in the member strength reduction. At 800 °C the strength is about 8% of that at room temperature, which is in contrast to three material reduction factors of K_y (800 °C) = 0.11, K_p (800 °C) = 0.05 and K_E (800 °C) = 0.09. The results for 800 °C are intended as an upper bound on the temperature response, since the large strength reduction at this temperature suggests that the practical value of calculating the strength at this temperature is limited. The beam data (Fig. 4(b)) are for a W14 × 22 beam with a lateral slenderness of $L/r_y = 60$ subjected to a uniformly distributed strong-axis moment. Here, the strengths reductions at elevated temperatures are slightly less than for the column, suggesting that the beam behavior is more dependent on the reduction in yield strength and less on the reduction in proportional limit. In these two examples, the arc-length (Riks) solution method is used to track the post-peak response. For the parametric studies shown later, where only the peak strength is reported, the finite element analyses were run under load control up to the critical strength limit state. This was done as a practical measure to reduce the analysis run times.

Analyses were also conducted to assess the effects of thermally-induced residual stresses and cross-section imperfections on critical loads. Residual stresses were introduced with the distribution shown in Fig. 5(a), assuming a peak residual stress at ambient temperature of $F_{r0} = 69$ MPa (10 ksi). Under elevated temperatures the peak residual stresses are assumed to reduce in proportion to the reduction in yield stress, i.e., $F_r(T) = K_y(T)F_{r0}$. Shown in Fig. 5(b) are critical column strengths obtained from simulations run with and without residual stresses at an elevated temperature of 500 °C. The largest difference occurs at a slenderness of about $L/r_y = 100$, where the residual stresses reduce the critical calculated load by less than 15%. Residual stresses are modeled in this same way for the subsequent parametric analyses presented later.

While the primary focus of this study is on compact or near-compact sections, the significance of local flange or web buckling and local geometric imperfections was considered.

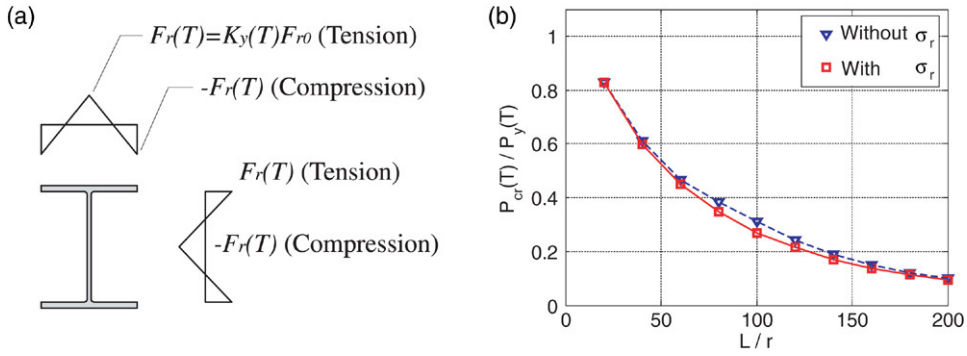

Fig. 5. Influence of residual stresses: (a) residual stress pattern, (b) critical weak-axis buckling strength of W14 × 90 Gr. 50 column at 500 °C.

Previous research has reported that local buckling is not particularly critical at elevated temperatures for structural sections, for which local buckling is not critical at ambient temperature [5–7]. This observation is corroborated by this study where local buckling was only observed as governing the strength limit state in a few of the FEM analyses of very short columns where the web width–thickness ratios exceed the AISC requirements for compact column sections. To help assess the significance of local geometric imperfections, a W14 × 90 (Grade 50) column of varying slenderness was analyzed with and without local imperfections at an elevated temperature of 500 °C. The local imperfections were defined by scaling the first-mode local buckling shape, obtained by a linear buckling analysis, to a maximum amplitude of 1/1000 of the local buckling length (equal to a peak flange and web imperfection of about 0.5–0.8 mm). Strength deterioration due to the local imperfection was only observed for the shorter members (lengths of 3.1 m for flexural buckling about the strong axis and 1.9 m for flexural buckling about the minor axis), where the maximum difference in critical strengths for analyses with and without the imperfection are 5% and 3% for flexural bucking about strong and weak axes, respectively. Thus, these analyses support the assumption that the member strengths are no more sensitive to local buckling at elevated temperatures as compared to ambient temperatures, and the response of compact (and near-compact) sections are fairly insensitive to local geometric imperfections.

4. Column strength assessment

Many numerical and experimental studies have been carried out on the behavior of steel columns under elevated temperatures [8–12]. Franssen et al. [13] used finite element techniques to numerically simulate column response under elevated temperatures and proposed new column design equations for EC3. Talamona et al. [14] and Franssen et al. [15] subsequently performed comprehensive analytical studies to investigate the critical temperatures for various I-shaped sections with varying slenderness ratios, yield stresses, member orientations, axial loads, and loading eccentricities. They used the critical axial column strengths from these analyses to confirm the proposed design equations by Franssen et al. [13]. The EC3 column design equations [1] have since been modified to incorporate the proposed revisions. These prior studies provide the impetus for this current study to independently assess the nominal strength provisions of the latest EC3 (2003) standard and the new AISC (2005) specification.

4.1. AISC column strength equations

The nominal column strength $P_{\text{cr0,AISC}}$ of the AISC specification at ambient temperature is calculated as follows:

$$\text{For } F_{y0} \le 2.25F_{e0} \qquad P_{\text{cr0,AISC}} = \left[0.658^{\frac{F_{y0}}{F_{e0}}}\right] AF_{y0} \tag{2}$$

$$\text{For } F_{y0} > 2.25F_{e0} \qquad P_{\text{cr0,AISC}} = 0.877AF_{e0} \tag{3}$$

where

$$F_{e0} = \frac{\pi^2 E_0}{\left(\frac{KL}{r}\right)^2} \tag{4}$$

where, F_{y0} and E_0 are the yield stress and elastic modulus; F_{e0} is elastic buckling stress, given by Eq. (4); and A, r, and K are cross-sectional area, radius of gyration, and effective buckling length factor, respectively.

The AISC equations for calculating the critical load at elevated temperatures, $P_{\text{cr,AISC}}(T)$, are identical to Eqs. (2)–(4), except that the elastic modulus and yield strength terms are replaced by their temperature dependent counterparts, $E(T)$ and $F_y(T)$, which are determined using the EC3 reduction factors of Eq. (1) and Table 1.

4.2. EC3 column strength equations

The EC3 column strength $P_{\text{cr0,EC3}}$ at ambient temperature is calculated as follows:

$$P_{\text{cr0,EC3}} = \chi_0 P_{y0} \tag{5}$$

$$\chi_0 = \frac{1}{\varphi_0 + \sqrt{\varphi_0^2 - \bar{\lambda}_0^2}} \le 1.0 \tag{6}$$

$$\varphi_0 = 0.5\left[1 + \alpha\left(\bar{\lambda}_0 - 0.2\right) + \bar{\lambda}_0^2\right] \tag{7}$$

$$\bar{\lambda}_0 = \sqrt{\frac{F_{y0}}{F_{e0}}} \tag{8}$$

Table 2
Steel section data

Section	h (mm)	t_w (mm)	b_f (mm)	t_f (mm)	h/t_w	$b_f/2t_f$	I_x/I_y
W14 × 90	356	11.2	369	18.0	25.9	10.3	2.8
W14 × 22	349	5.8	127	8.5	53.7	7.47	28.4
HEA100	96	5	100	8	19.2	5.0	2.5

where α is an imperfection factor, which varies from 0.13 to 0.76 depending on the member properties, such as buckling orientation (i.e. about the weak axis or strong axis), web height to flange width ratio, flange thickness, and yield stress. $\bar{\lambda}_0$ is a slenderness ratio that is given by Eq. (8) for stocky sections (i.e. Class 1, Class 2, or Class 3 cross-sections, as defined in EC3) and the other parameters are as defined previously. One of the notable differences between the AISC and EC3 equations is that the critical load in EC3 depends on the slenderness ratio, buckling axis, and cross section properties, whereas the AISC strength only varies with respect to the flexural slenderness ratio, KL/r.

Design equations at elevated temperatures in EC3 are similar to the ones at ambient temperature, but with a few important differences. Equations for critical load $P_{\mathrm{cr,EC3}}(T)$ are the same as Eqs. (5) and (6), except that the yield strength of Eq. (5) is replaced by its temperature dependent counterpart, $P_y(T)$, as specified using the yield strength reduction factor of Table 1 and Fig. 2(c). At elevated temperatures, $\chi(T)$ is calculated by Eq. (6) but with the following temperature dependent parameters that replace the expressions in Eqs. (7) and (8):

$$\varphi(T) = 0.5\left[1 + \alpha\bar{\lambda}(T) + \bar{\lambda}^2(T)\right] \tag{9}$$

$$\bar{\lambda}(T) = \bar{\lambda}_0\sqrt{\frac{K_y(T)}{K_E(T)}} \tag{10}$$

$$\alpha = 0.65\sqrt{235/F_{y0}} \tag{11}$$

where $\bar{\lambda}_0$ is as specified in Eq. (8) and $K_y(T)$ and $K_E(T)$ are the reduction factors of Table 1 and Fig. 2(c).

4.3. Assessment of column strengths

The AISC and EC3 column strength equations are compared to FEM simulations of two column sections under various temperatures and slenderness ratio. The columns consist of W14 × 22 and W14 × 90 sections with Gr. 50 and 36 steels (W360 × 32.9 and W360 × 134 sections with F_y = 345 MPa and 250 MPa). Member section properties are summarized in Table 2, where h, t_w, b_f and t_f are the height, web thickness, flange width and flange thickness, respectively. As is evident from the ratio of strong to weak axis moment of inertia, I_x/I_y, the W14 × 22 represents a beam type geometry, whereas the W14 × 90 represents a column geometry. Per EC3, the imperfection factors for these cross sections are $\alpha_x = 0.21$ and $\alpha_y = 0.34$.

The AISC characterizes column cross sections by the width to thickness ratios of the flanges and webs to denote the transition between sections that are expected to be controlled by local flange or web buckling prior to section yielding. Referring to Table 2, both of the W14 sections satisfy the AISC criteria for compact flanges of $b_f/2t_f < 13.5$ and 15.8 for Gr. 50 and 36 steel, respectively. On the other hand, the web slenderness of the W14 × 22 section (h/t_w = 53.7) exceeds the limiting AISC compactness criteria of h/t_w = 35.9 and 42.1 for Gr. 50 and 36 steel, respectively. Therefore, these data indicate that the W14 × 22 is expected to be sensitive to local web buckling at high stresses, whereas other local buckling modes should not affect the results. These two W14 sections are intended to represent the range of behavior for rolled wide-flange members encountered in design practice.

Superimposed in Fig. 6(a) are FEM simulation results and nominal strengths calculated according to the AISC and EC3 provisions for the W14 × 90 (Gr. 50) column at ambient temperature. These results are shown as a benchmark against which to judge the differences in the models at elevated temperatures. Critical strengths of members were investigated for elevated temperature increments of 100 °C up to 800 °C. Representative results are shown in Fig. 6(b)–(d) for temperatures of 200, 500 and 800 °C. As noted previously, the results at 800 °C have limited practical impact but are included to show the bounds of response. Simulation (ABAQUS) results are shown for both strong and weak axis buckling for slenderness ratios from 20 to 200. Compared to the ambient temperature case, the differences between simulated results for strong versus weak axes decrease at higher temperatures. Clearly evident in these figures is that the AISC strength equations are unconservative at elevated temperatures, particularly for slenderness ratios between 40 and 100 and temperatures above 500 °C. For instance, referring to the strength ratio comparisons in Fig. 7, at 500 °C the nominal strengths calculated by the AISC provisions are up to 60% larger than the critical strengths as calculated by simulation. On the other hand, the EC3 column strength equations match the simulated results within about 20%.

4.4. Proposed column strength equations

Motivated by the large discrepancy between the AISC provisions and the simulated results, the authors developed an alternative column strength equation that is similar in format to the AISC equations but with greatly improved accuracy at high temperatures. The proposal is to use the following equation for elevated temperatures in lieu of Eqs. (2) and (3):

$$P_{\mathrm{cr,Prop}}(T) = \left[0.42^{\sqrt{\frac{F_y(T)}{F_e(T)}}}\right] AF_y(T) \tag{12}$$

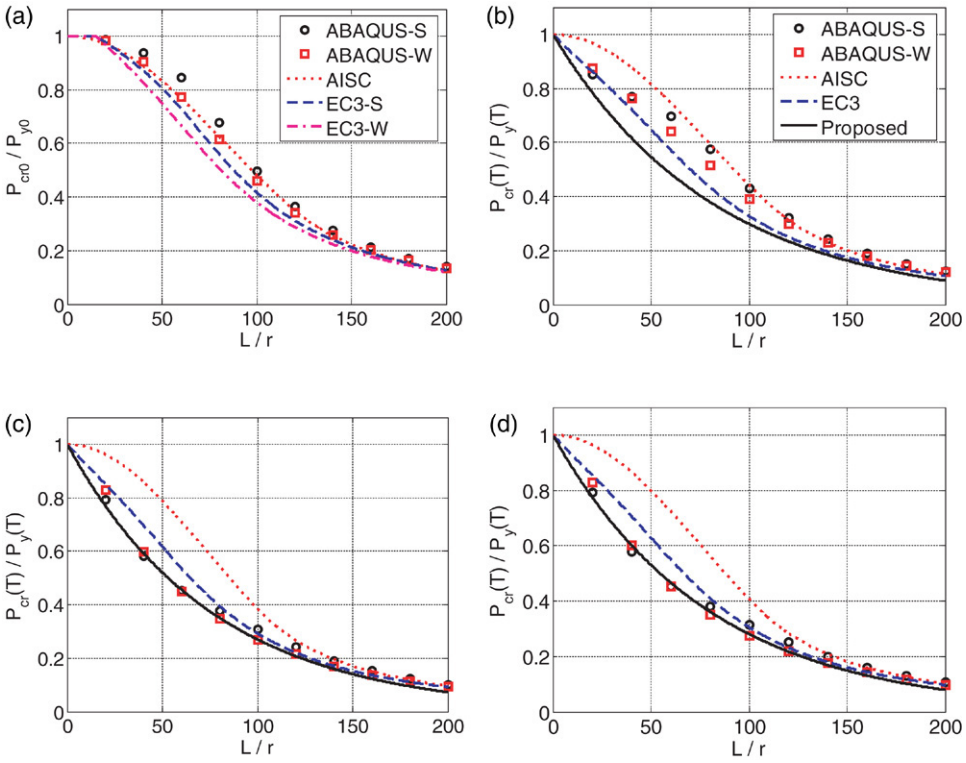

Fig. 6. Critical compressive strengths of W14 × 90 Gr. 50 column, (a) ambient temperature, (b) 200 °C, (c) 500 °C, (d) 800 °C.

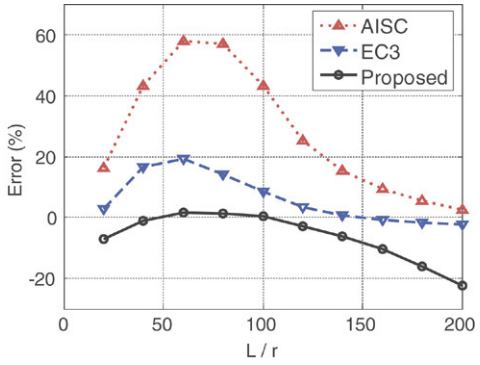

Fig. 7. Percent error in the calculated compression strength of W14 × 90 Gr. 50 column at 500 °C.

where

$$F_e(T) = \frac{\pi^2 E(T)}{\left(\frac{KL}{r}\right)^2}. \tag{13}$$

This equation is similar to the AISC equation (2) but with a different coefficient and exponent. Like the AISC equations, this model utilizes the EC3 reduction factors to calculate $F_y(T)$ and $E(T)$. As compared with other data in Figs. 6(b)–(d) and 7, the nominal strength by the proposed equations track the simulation data fairly well, closer in fact that than the EC3 equations at temperatures greater than 300 to 400 °C, where structural fire analyses are important.

4.5. Column test data

To further substantiate these analyses, results of the finite element simulations and nominal strengths are compared to test data reported by Franssen et al. [15]. The column tests were of a HEA100 section, whose sizes are shown in Table 2. Data for five column tests at varying temperatures and lengths are summarized in Table 3 along with results from finite element simulations and the three nominal equations (AISC, EC3, and the newly proposed equations). Measured steel yield strengths at ambient temperature (as reported by Franssen et al.) were used for F_{y0} in the analytical simulations and strength equations. Flexural buckling about the weak axis was the dominant mode of failure in all cases. Referring to Table 3, four of the five finite element simulations predict strengths within 3% of the measured strengths, thus confirming the validity of the simulations as a basis for evaluating the design models. Critical strengths calculated by EC3 are all within 30% of the test data, whereas those by the AISC equations are unconservative by up to 65%. Strengths predicted using the proposed equations are within 10% of the measured test data.

4.6. Influence of yield strength and section geometry

Results of analyses to examine the influence of yield strength and section properties are shown in Fig. 8(a)–(b). Comparing Fig. 8(a) to 6(c), the trends in both the simulation and relative accuracy of the design equations is essentially the same for Gr. 36 as Gr. 50 steel. The influence of section proportions (W14 × 22 versus W14 × 90) is seen by comparing Figs. 8(b)

Table 3
Measured and calculated strengths of column tests

Test name	L/r_y	T (°C)	P_{cr} (kN) ($P_{cr}/P_{cr,Test}$)				
			Test	FEM	AISC	EC3	Proposed
CL1	20	694	110	107 (0.97)	142 (1.29)	123 (1.12)	112 (1.02)
CL3	50	474	251	244 (0.97)	414 (1.65)	320 (1.27)	277 (1.10)
SL40	79	525	170	143 (0.84)	250 (1.47)	177 (1.04)	159 (0.94)
AL5	108	457	127	131 (1.03)	198 (1.56)	145 (1.14)	138 (1.09)
BL6	137	446	105	103 (0.98)	125 (1.19)	104 (0.99)	100 (0.95)

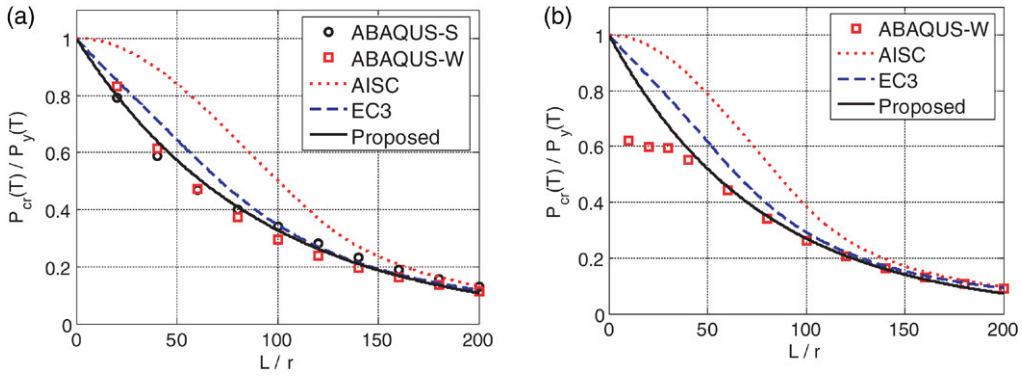

Fig. 8. Comparative assessment of column compression strength at 500 °C (a) W14 × 90 Gr. 36, (b) W14 × 22 Gr. 50.

and 6(c). For the W14 × 22 only minor axis flexural buckling is considered due to the large difference in strong versus weak axis properties. In Fig. 8(b) the effect of web slenderness web in the W14 × 22 is apparent, where the simulated results drop off compared to the design equations at low slenderness ($L/r < 30$) where the critical stress exceeds about $0.6F_y(T)$. This occurs because at these stress levels local web buckling, which is not reflected in the column strength equations, begins to control the critical strength. It turns out that for this column, these discrepancies are not of much practical significance since the column length corresponding to $L/r = 30$ is only 0.80 m. Except for these cases where web buckling is critical (and is expected based on the fact that the h/t_w exceeds the AISC limit for compact webs), the critical strengths agree well with the proposed equation. Additional analyses of the W14 × 22 section at other temperatures confirm that the critical web buckling stress of about $0.6F_y(T)$ is fairly constant across various temperature ranges.

5. Beam strength assessment

Design equations for laterally unsupported beams require evaluation of torsional–flexural instability effects, which for I-shaped sections involves consideration of non-uniform torsion and warping restraint. Compared to columns and laterally supported beams, there are relatively few studies of laterally unsupported beams under fire conditions. Bailey et al. [16] studied the critical temperatures for several beam sections with different loading patterns and commented that the then current EC3 provisions were unconservative for laterally unsupported beams. Piloto and Vila Real [17] performed an experimental study of electronically heated beams and reported that the measured critical temperatures were scattered and generally higher than the theoretical or design temperatures. They attributed the variations to the complexity of the phenomena and the difficulty in conducting the experiments. Vila Real et al. [18–20] numerically studied the critical temperatures and strength for various loading patterns, from which they proposed alternative design equations that were later incorporated in EC3 [1].

Building upon prior research, analytical results for laterally unsupported beams are compared with design equations of the AISC and EC3 specifications, similar to the column comparisons. As in the column study, the large discrepancy between the AISC strength equations and simulation results prompted the proposal of alternative equations for evaluating beams at elevated temperatures.

5.1. AISC beam strength equations

The AISC equations for beam strength at ambient temperature are given by the following equations, where M_{p0} is the plastic moment and M_{r0} is the initial yield moment (reduced to account for residual stresses), E_0 and G_0 are the elastic moduli, J is the torsional constant, C_w is the warping constant, and λ is the slenderness ratio ($=L/r_y$):

For $\lambda \le \lambda_{p0}$ $\quad M_{cr0,AISC} = M_{p0}$ (14)

For $\lambda_{p0} < \lambda \le \lambda_{r0}$

$$M_{cr0,AISC} = M_{p0} - (M_{p0} - M_{r0})\left(\frac{\lambda - \lambda_{p0}}{\lambda_{r0} - \lambda_{p0}}\right) \quad (15)$$

For $\lambda > \lambda_{r0}$

$$M_{\text{cr0,AISC}} = \frac{\pi}{\lambda r_y}\sqrt{E_0 I_y G_0 J + I_y C_w \left(\frac{\pi E_0}{\lambda r_y}\right)^2}. \quad (16)$$

The slenderness ratios, λ_{p0} and λ_{r0}, correspond to the transitions between full plastic bending capacity, inelastic lateral–torsional buckling, and elastic lateral–torsional buckling, represented by Eqs. (14), (15) and (16), respectively. λ_{p0} is determined from empirical data, while λ_{r0} corresponds to the theoretical slenderness where the critical elastic buckling moment, per Eq. (16), is equal to the initial yield moment M_{ro}. The critical moment for elastic lateral torsional buckling with Eq. (16) is theoretically derived (Timoshenko and Gere [21]) and that for inelastic buckling with Eq. (15) is a linear interpolation between the transition points with Eqs. (14) and (16). These transition points are calculated by the following equations, where S_x is the elastic section modulus about the strong axis and the other terms are as defined previously:

$$\lambda_{p0} = 1.76\sqrt{\frac{E_0}{F_{y0}}} \quad (17)$$

$$\lambda_{r0} = \frac{X_{10}}{F_{L0}}\sqrt{1+\sqrt{1+X_2 F_{L0}^2}} \quad (18)$$

$$M_{r0} = S_x F_{L0} \quad (19)$$

where

$$X_{10} = \frac{\pi}{S_x}\sqrt{\frac{E_0 G_0 J A}{2}} \quad (20)$$

$$X_2 = 4\frac{C_w}{I_y}\left(\frac{S_x}{GJ}\right)^2 \quad (21)$$

$$F_{L0} = 0.7F_{y0}. \quad (22)$$

As specified in AISC [2], the critical moment under elevated temperatures $M_{\text{cr,AISC}}(T)$ is obtained from Eqs. (14) to (21) by modifying E, G and F_y using the reduction coefficients $K_E(T)$ and $K_y(T)$.

5.2. EC3 beam strength equations

The EC3 beam strength equations at ambient temperature have a similar format to the EC3 column equations:

$$M_{\text{cr0,EC3}} = \chi_{LT0} M_{p0} \quad (23)$$

$$\chi_{LT0} = \frac{1}{\varphi_{LT0} + \sqrt{\varphi_{LT0}^2 - \bar{\lambda}_{LT0}^2}} \le 1.0 \quad (24)$$

where

$$\varphi_{LT0} = 0.5\left[1 + \alpha_{LT}(\bar{\lambda}_{LT0} - 0.2) + \bar{\lambda}_{LT0}^2\right] \quad (25)$$

$$\bar{\lambda}_{LT0} = \sqrt{\frac{M_{p0}}{M_{\text{cr0},e}}} \quad (26)$$

$$M_{p0} = Z_x F_{y0} \quad (27)$$

and χ_{LT0} is the reduction factor for lateral torsional buckling, α_{LT} is an imperfection factor which depends on the section proportions ($\alpha_{LT} = 0.21$ is used for rolled sections with the web height to flange width ratio $h/b_f \le 2$ and $\alpha_{LT} = 0.34$ for $h/b_f > 2$), $M_{\text{cr0},e}$ is the elastic critical moment for lateral torsional buckling, and Z_x is the plastic modulus about the strong axis. Eq. (26) is specified for compact sections, which correspond to the Class 1 or Class 2 designations in EC3.

Differences between the beam equations in EC3 under fire conditions and at ambient temperature are similar to those between the corresponding column equations. The primary changes are in the definition of φ_{LT}, α_{LT}, and $\bar{\lambda}_{LT}$, which are defined for elevated temperatures by the following equations that replace Eqs. (25)–(27):

$$\varphi_{LT}(T) = 0.5\left[1 + \alpha_{LT}\bar{\lambda}_{LT}(T) + \bar{\lambda}_{LT}^2(T)\right] \quad (28)$$

$$\alpha_{LT} = 0.65\sqrt{235/F_{y0}} \quad (29)$$

$$\bar{\lambda}_{LT}(T) = \bar{\lambda}_{LT0}\sqrt{\frac{K_y(T)}{K_E(T)}}. \quad (30)$$

Note that F_{y0} carries units of MPa in Eq. (29).

5.3. Proposed beam strength equations

As an alternative to the AISC beam strength equations, the following equations are proposed to evaluate bending strengths at elevated temperatures using a similar format to the AISC design equations:

$$\text{For } \lambda \le \lambda_r(T) \qquad M_{\text{cr,Prop}}(T) = M_r(T) + [M_p(T) - M_r(T)]\left(1 - \frac{\lambda}{\lambda_r(T)}\right)^{C_X(T)} \quad (31)$$

$$\text{For } \lambda > \lambda_r(T) \qquad M_{\text{cr,Prop}}(T) = \frac{\pi}{\lambda r_y}\sqrt{E(T) I_y G(T) J + I_y C_w \left(\frac{\pi E(T)}{\lambda r_y}\right)^2}. \quad (32)$$

In contrast to the equations at ambient temperature where the design equations are distinguished into three regions of behavior, here only two equations are used to model inelastic and elastic lateral–torsional buckling. As will be shown later, these equations reflect that fact that at elevated temperatures the critical moment drops off quickly from the plastic moment at small slenderness values. The distinction between inelastic and elastic behavior is indicated by the slenderness value $\lambda_r(T)$, which corresponds to the elastic moment at the onset of yielding, $M_r(T)$. The governing equations for $\lambda_r(T)$ and $M_r(T)$ are the same as the AISC values, Eqs. (18)–(22) with reduced yield stress and elastic modulus, except that the initial yield stress F_L is replaced by the following:

$$F_L(T) = F_p(T) - F_r(T) \quad (33)$$

$$F_p(T) = K_p(T) F_{y0} \quad (34)$$

$$F_r(T) = K_y(T) F_{r0}. \quad (35)$$

Compared to the original AISC equations, the major change is to base $F_L(T)$ on the temperature dependent proportional limit

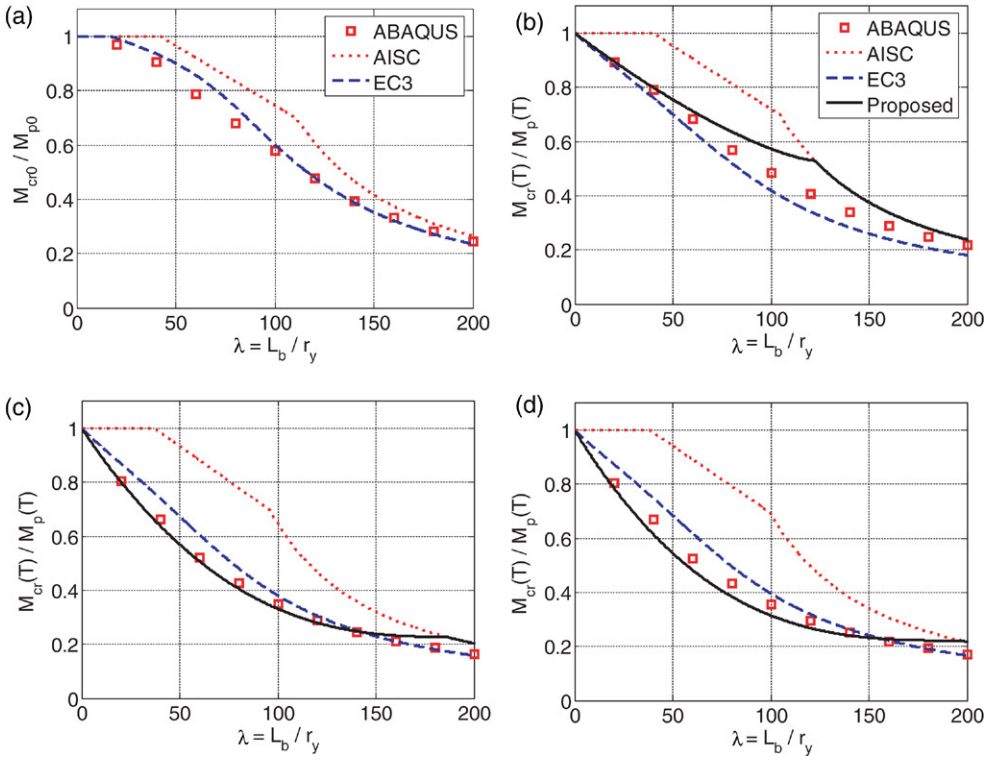

Fig. 9. Critical bending moment strengths of W14 × 22 Gr. 50 beam, (a) ambient temperature, (b) 200 °C, (c) 500 °C, (d) 800 °C.

$F_p(T)$ rather than the yield stress. F_{r0} is the residual stress at the ambient temperature, which is specified in AISC as $F_{r0} =$ 69 MPa for rolled shapes. Implied in Eq. (35) is the assumption that the residual stresses under elevated temperatures are proportional to the reduction factor of yield strength, $K_y(T)$. The term $C_X(T)$ in Eq. (31) is an exponent that is defined as a bilinear function with respect to the temperature according to the following equation for $T > 100$ °C,

$$C_X(T) = 0.6 + \frac{T}{250} \leq 3.0 \tag{36}$$

where T carries units of °C.

5.4. Assessment of beam strengths

Comparisons between the simulated results and design equations for bending strength are shown in Figs. 9 through 11. Simulated results for a W14 × 22 Gr. 50 ($F_y = 345$ MPa) beam of varying lateral slenderness are compared to the AISC and EC3 equations at ambient temperatures in Fig. 9(a). As in the column analyses, the simulated points correspond to the peak point in load versus deflection curves, such as shown previously in Fig. 4(b). The comparison in Fig. 9(a) demonstrates that even at ambient temperatures, the AISC flexure equations tend to be unconservative relative to the simulated results and EC3 equations. In this example, the maximum error occurs at an intermediate slenderness, $\lambda = 100$, where the AISC strength is about 30% larger than the simulated results.

Strengths for the W14 × 22 beam at elevated temperatures, 200, 500 and 800 °C, are compared in Fig. 9(b)–(d). Included are the FEM simulation results and the nominal strengths calculated by the three design equations (AISC, EC3, and the proposed model). Immediately apparent from these comparisons are the large discrepancies between the AISC equations and the simulated results. Referring to Fig. 10, at 500 °C the largest percentage differences occur for intermediate slenderness values of $\lambda = 80$–100, where the AISC strengths are about 80% higher than the simulated strengths at temperatures. In part, the discrepancies arise because at elevated temperatures the simulated results indicate that the moment strength drops off quickly with increasing slenderness, whereas the AISC equations preserve the plastic moment, $M_p(T)$, up to about $\lambda = 40$. In contrast to the AISC equations, the EC3 model tracks the simulated results fairly well.

As indicated previously, the new equations proposed by the authors are intended to provide good accuracy while maintaining a similar concept and format to the AISC equations. One of the basic features of the proposed model is that it preserves use of the elastic critical load at high slenderness values. At lower temperatures (e.g., 200 °C) the transition between the inelastic and elastic response, at $\lambda = 110$, is quite abrupt. At higher temperature, as the proportional limit is reduced through $K_p(T)$, the inelastic curve controls over a larger range of slenderness. As evident from Figs. 9(c)–(d) and 10, at above about 300 °C results from the proposed model and the EC3 model are quite similar and agree well with the simulation data. The proposed model is less conservative than the EC3 equations at lower temperatures (e.g., 200 °C in Fig. 9(b)), owing to the desire to maintain

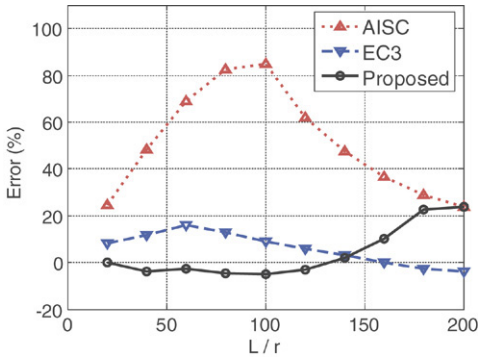

Fig. 10. Percentage error in the calculated bending moment strength of W14 × 22 Gr. 50 beam at 500 °C.

close conformance with the AISC relationships at ambient temperature.

Results shown in Fig. 11 illustrate that the trends observed in Fig. 9 for the W14×22 Gr. 50 beam are generally representative of other yield strengths and section properties. Results for Gr. 36 steel ($F_y = 250$ MPa) at 500 °C are shown in Fig. 11(a). Here the effect of the residual stresses (assumed at $F_{r0} = 69$ MPa at ambient temperature) are proportionally larger for the Gr. 36 steel, and the increased softening effect leads to closer agreement between the EC3 and proposed equations, as compared to the results shown in Fig. 9(c) for Gr. 50 steel. Results for a W14 × 90 Gr. 50 beam at 500 °C are shown in Fig. 11(b) . In this case, the strengths calculated by the EC3 and proposed models agree very well with the simulated results up to about $\lambda = 100$. At higher slenderness these two models tend to underestimate the critical load, because the proportions of the W14 × 90 (smaller I_x/I_y ratio) are such that the in-plane pre-buckling deformations tend to increase the critical load. This beneficial effect of in-plane deflections is picked up in the simulation but not in the critical load equations. Overall, the results in Fig. 11 confirm that the EC3 and the proposed models provide accurate results for the typical range of steel shapes and yield strengths used in practice.

6. Beam–column strength assessment

Laterally unsupported beam–columns subjected to combined axial compression and strong axis bending experience combined limit states of yielding, lateral buckling and lateral torsional buckling. As with laterally unsupported beams, there are relatively few studies of design equations for beam–columns under fire conditions. Lopes et al. [22] compared numerical simulations to equations in the 1995 and 2003 editions of EC3 and confirmed that the 2003 provisions are more accurate and conservative than the 1995 provisions. Toh et al. [11] proposed an approach to find combinations of the critical axial force and bending moment using Rankin's method. In the following discussion, results of the present study of columns and beams is extended to evaluate the AISC and EC3 design equations for beam–columns subjected to axial load and major-axis bending.

6.1. AISC beam–column strength equations

The AISC beam–column strength equations employ a simple bilinear combination of the ratio of axial and bending effects. As given by the following, the equations for elevated temperatures are identical to those at ambient temperatures except that the nominal strengths are calculated at elevated temperatures:

$$\text{For } \frac{P_u}{P_{\text{cry,AISC}}(T)} \geq 0.2$$

$$\frac{P_u}{P_{\text{cry,AISC}}(T)} + \frac{8}{9}\frac{M_{ux}}{M_{\text{crx,AISC}}(T)} \leq 1.0 \tag{37}$$

$$\text{For } \frac{P_u}{P_{\text{cry,AISC}}(T)} < 0.2$$

$$\frac{P_u}{2P_{\text{cry,AISC}}(T)} + \frac{M_{ux}}{M_{\text{crx,AISC}}(T)} \leq 1.0 \tag{38}$$

where P_u and M_{ux} are the factored axial load and bending moment about the strong axis and $P_{\text{cry,AISC}}(T)$ and $M_{\text{crx,AISC}}(T)$ are the critical axial strength for flexural buckling and the critical bending moment for lateral torsional buckling, respectively. Assuming the member to be pin-ended about both axes, the column strength $P_{\text{cry,AISC}}(T)$ is controlled by flexural buckling about the weak axis. Per the AISC Specification, M_{ux} should include second-order effects. For the pin-ended column subjected to uniform end moments, $M_{x,\text{end}}$, the second-order

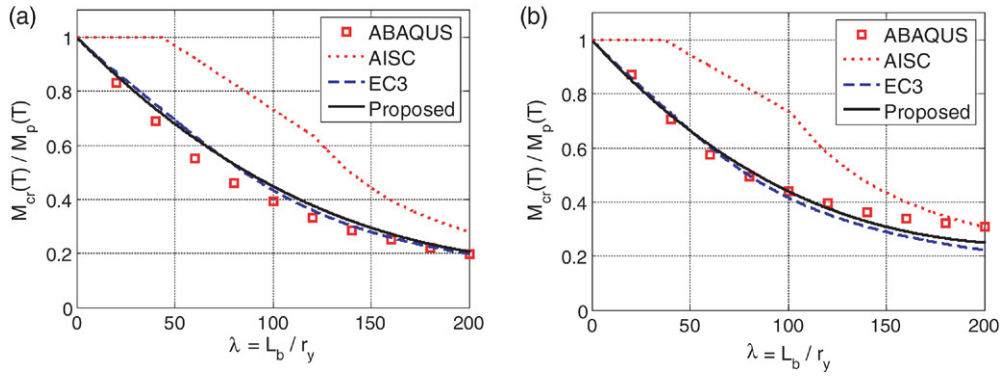

Fig. 11. Comparative assessment of beam bending moment strength at 500 °C (a) W14 × 22 Gr. 36, (b) W14 × 90 Gr. 50.

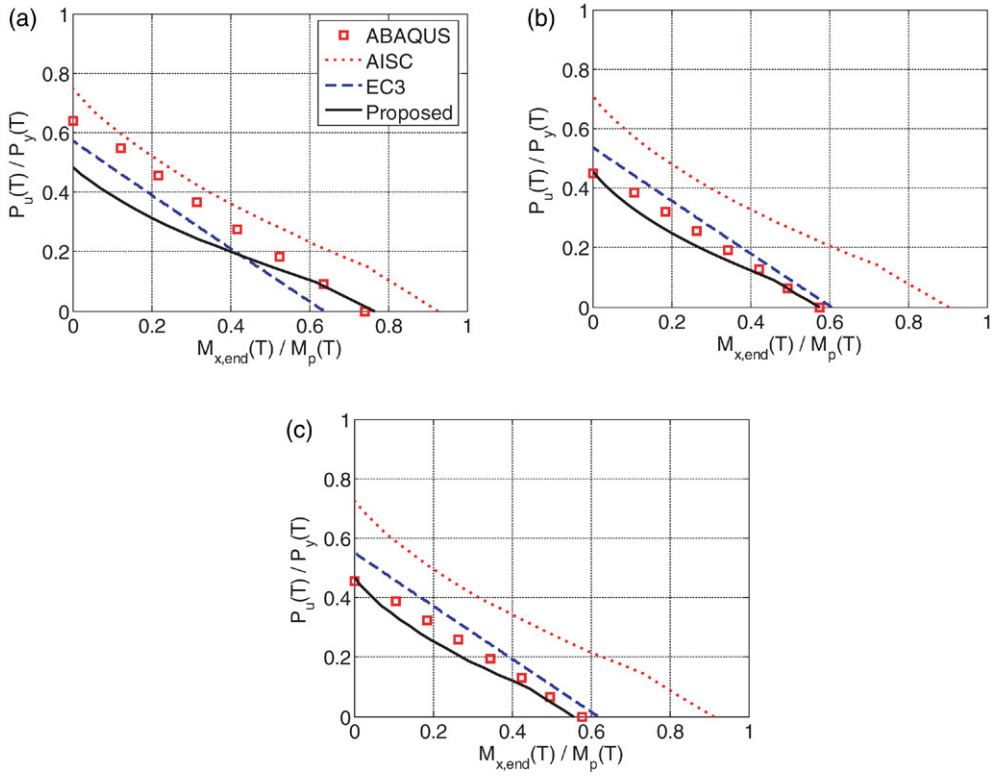

Fig. 12. Critical axial load and moment strengths of W14 × 90 Gr. 50 (λ = 60) beam–column, (a) 200 °C, (b) 500 °C, (c) 800 °C.

moment at the mid-span is calculated as:

$$M_{ux}(T) = \frac{M_{x,\text{end}}}{1 - P_u/P_{\text{cr},e}(T)} \tag{39}$$

where

$$P_{\text{cr},e}(T) = \frac{\pi^2 E(T) A}{\lambda^2}. \tag{40}$$

According to Eq. (39), the second-order amplification factor is calculated based on the critical load determined using $E(T)$ and per Eq. (1).

6.2. Proposed beam–column strength equations

The proposed equations employ the same interaction check and amplification factor as the AISC equations, except that the nominal strength terms, $P_{\text{cry,Prop}}(T)$ and $M_{\text{cry,Prop}}(T)$, are calculated according to the newly proposed equations.

6.3. EC3 Beam–column strength equations

The EC3 beam–column equations for combined axial load and bending moment are as follows:

$$\frac{P_u}{P_{\text{cry,EC3}}(T)} + k_{LT}(T)\frac{M_{ux}(T)}{M_{\text{cr,EC3}}(T)} \le 1.0 \tag{41}$$

where,

$$P_{\text{cry,EC3}}(T) = \chi_y(T) P_y(T) \tag{42}$$

$$k_{LT}(T) = 1 - \mu_{LT}(T)\frac{P_u}{P_{\text{cry,EC3}}(T)} \tag{43}$$

$$\mu_{LT}(T) = 0.165\bar{\lambda}_y(T) - 0.15 \le 0.9 \tag{44}$$

where P_u and $M_{ux}(T)$ are the factored axial load and bending moment about the strong axis and $P_{\text{cr,EC3}}(T)$ and $M_{\text{cr,EC3}}(T)$ are the critical axial strength for flexural buckling and the critical bending moment for lateral torsional buckling, respectively, and other terms are as defined previously. Note that Eq. (44) for $\mu_{LT}(T)$ is shown in simplified format for a pin-ended beam–column subjected to uniform end moments.

6.4. Assessment of beam–column strengths

The same FEM analysis model used for the column and beam studies is used for beam–column study, including non-uniform torsion and warping restraint effects. The limit state combinations of axial load versus end moment are compared in Fig. 12 for a W14 × 90 (Gr. 50) member with λ = 60 at various elevated temperatures. The curve in the AISC and proposed equations is due to the second-order effects in $M_{ux}(T)$ per Eq. (39). In general both the EC3 and proposed equations show good agreement with the simulated results. It is difficult to say whether the bi-linear or linear interaction equations are more appropriate, since much of the accuracy of the interaction check depends on the accuracy of the nominal axial load and moment strength. Following the previous discussion of the axial load and moment strengths, the AISC provisions at elevated temperatures are highly unconservative relative to the simulated

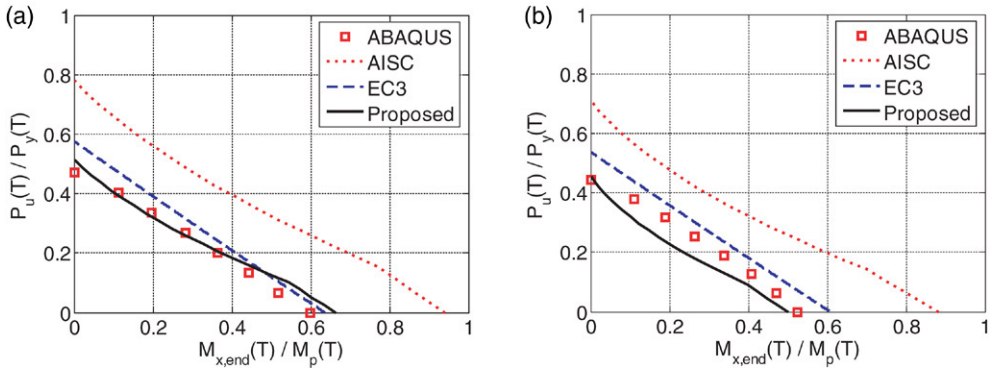

Fig. 13. Comparative assessment of beam–column strengths at 500 °C (a) W14 × 9043 Gr. 36, (b) W14 × 22 Gr. 50.

results and other design equations. The errors are larger for bending dominated (as opposed to axial dominated) members, owing to the underlying errors in the $M_{cr,AISC}(T)$ equations discussed previously.

Results in Fig. 13 illustrate similar results for a lower yield steel strength and alternative steel section. Comparing Figs. 12(b) and 13(a), the differences between Gr. 50 and Gr. 36 steel at 500 °C indicate that results from the simulation, EC3 and proposed equations tend to converge for Gr. 36 steel, presumably because the residual stresses and non-proportional limit are closer together. Conversely, the AISC results, which do not take into account the reduced proportional limit lose accuracy for Gr. 36. Comparing Figs. 12(b) and 13(b), the differences between the W14 × 90 to W14 × 22 sections lead to minor changes that can be traced back to differences in the axial load and moment strengths.

7. Summary and conclusions

Codified design equations for steel members subjected to high temperatures are an important step towards facilitating consensus standards to evaluate the structural safety of buildings to fire. Incorporation of fire provisions in structural design standards also raises awareness of the issues and has encouraged research and development to validate and improve the provisions. Design equations first introduced in the Eurocode EC3 standard in 1992 were subsequently updated and improved through studies by a number of researchers. Similar design requirements have only recently been introduced in a new appendix to the 2005 AISC Specification.

The results summarized herein provide an independent assessment of the EC3 and AISC provisions for columns, laterally unbraced beams, and laterally unbraced beam–columns, which are compared to data from detailed nonlinear finite element analyses. Utilizing three-dimensional shell finite elements, the numerical simulations incorporate the effects of local and overall buckling and instability, including non-uniform torsion and warping restraint effects. The simulation results are not entirely independent of the design standards, since the simulation models are based on stress–strain data at elevated temperatures that is specified in EC3 and referenced in AISC. However, through comparisons between the EC3 stress–strain models and test data of steel at elevated temperatures and column tests, the authors have reaffirmed the accuracy of the EC3 stress strain data. The simulation study included about four hundred finite element analyses, including the effects of varying slenderness, steel temperature, steel yield strength, residual stresses, and section properties.

Comparison between the AISC provisions and the simulation results indicate that the AISC provisions significantly over-estimate the nominal strength of columns, beams and beam–columns at elevated temperatures. The AISC column strengths were up to 60% higher than the simulated results, and the beam and beam–column strengths were 80%–100% higher. These large discrepancies indicate that the approach used in the AISC provisions of simply modifying the elastic moduli (E and G) and yield strength (F_y) in the otherwise standard (ambient temperature) design equations is inaccurate. Thus, the large variations are due primarily to the fact that the steel stress–strain curve loses its characteristic bi-linear elastic–plastic response at elevated temperatures. Comparisons between the EC3 provisions and simulation results indicate that the EC3 equations are within 20% of the simulations. This good agreement reflects refinements made to the EC3 provisions since their first publication.

While it would be tempting to simply recommend that the EC3 provisions be adopted into the AISC Specification, the format of the EC3 provisions is quite different from the AISC ambient strength design provisions. In the interest of maintaining similarity in format and style between ambient and elevated temperature provisions in the AISC Specification, new design equations are proposed as alternatives to those in the 2005 edition of the AISC specification. The proposed alternative equations for calculating the nominal column and beam strengths are validated against the simulation data and reduce the discrepancies to less than about 20%–30%, which is similar to the accuracy of the EC3 provisions. While similar in format, the proposed equations are distinct from the AISC provisions for ambient temperatures, and thus there is a discontinuity in response between the two sets of equations. The proposed equations are only intended for use at elevated temperatures, which can be assumed as temperatures higher than 200 °C, a temperature that would rarely if ever be exceeded except under fire conditions.

8. Limitations and future research

While this study helps to both validate and improve current design provisions for steel members at elevated temperatures, the scope is limited to assessment of individual members comprised of bi-symmetric I-shaped members with compact (or near-compact) sections. The current study treats the problem deterministically, using nominal properties (material strengths, initial imperfections, etc.) and nominal high-temperature material response parameters from EC3, whereas the actual conditions involve considerable uncertainty. Moreover, the current study assumes a uniform temperature distribution through the member cross section, which may not be conservative for slender members where non-uniform temperatures can induce member deformations that may accentuate destabilizing geometric nonlinear effects, i.e., moments induced by P–δ action (e.g., see Wang [5]). Finally, the current study is limited to evaluating the structural response, conditioned on the induced fire temperature, which ignores the challenges and large uncertainties in predicting the elevated temperatures and other fire effects.

Among the many areas that are ripe for future research and development, two areas most in need of further study are reliability analysis of uncertainties and the evaluation of indeterminate system response. The first of these should address a broader range of design and response parameters, including variations in cross-section types, thermal and mechanical loading intensities and distributions, material properties at ambient and elevated temperatures, and temperature induced distortions. The second topic would extend the assessment of individual components to assess collapse safety of indeterminate systems, considering the nonlinear redistribution of forces and the associated uncertainties in loading and response effects.

Acknowledgements

The authors gratefully acknowledge graduate fellowship support for the first author provided by the Fulbright Program and the John A. Blume Earthquake Engineering Center at Stanford University. Professor Vila Real P.M.M., University of Aveiro, Portugal, is greatly appreciated for the essential information regarding modern Eurocode 3 standard. The authors also appreciate discussions on structural fire engineering with members of the AISC Specification Task Committee on Thermal Effects as well as Barbara Lane and Susan Lamont of Arup.

References

[1] European Committee for Standardisation (CEN). Eurocode 3. Design of steel structures — part 1–2. General rules — structural fire design. Draft prEN 1993-1-2, Stage 49 Draft. Brussels (Belgium); 2003.

[2] American Institute of Steel Construction, Inc. (AISC). Specification for structural steel buildings. Chicago (IL); 2005.

[3] Wainman DE, Kirby BR. Compendium of UK standard fire test data, unprotected structural steel — 2. Ref. No. RS/RSC/S1199/8/88/B, British Steel Corporation (now Corus), Swinden Laboratories, Rotherham; 1988.

[4] Hibbitt, Karlsson & Sorensen. ABAQUS Version 6.3, User's manual. Hibbitt, Karlsson & Sorensen, Inc; 2002.

[5] Wang YC. Steel and composite structures behaviour and design for fire safety. Spon Press; 2002.

[6] Uy B, Bradford MA. Local buckling of cold formed steel in composite structural elements at elevated temperatures. Journal of Constructional Steel Research 1995;34:53–73.

[7] Ranby A. Structural fire design of thin walled steel sections. Journal of Constructional Steel Research 1998;46(1–3):303–4.

[8] Burgess IW, Olawale AO, Plank RJ. Failure of steel columns in fire. Fire Safety Journal 1992;18:183–201.

[9] Poh KW, Bennetts ID. Behavior of steel columns at elevated temperatures. Journal of Structural Engineering 1995;121(4):676–84.

[10] Talamona D, Kruppa J, Franssen JM, Recho N. Factors influencing the behaviour of steel columns exposed to fire. Journal of Fire Protection Engineers 1996;8(1):31–43.

[11] Toh WS, Tan KH, Fung TC. Compressive resistance of steel columns in fire: Rankine approach. Journal of Structural Engineering 2000;126(3): 398–405.

[12] Baker DJ, Xie YM, Dayawansa PH. Numerical predictions and experimental observations of the structural response of steel columns to high temperatures. In: Fire safety science, proceedings of the fifth international symposium. 1997. p. 1165–76.

[13] Franssen JM, Schleich JB, Cajot LG. A simple model for the fire resistance of axially loaded members according to Eurocode 3. Journal of Constructional Steel Research 1995;35:49–69.

[14] Talamona D, Franssen JM, Schleich JB, Kruppa J. Stability of steel columns in case of fire: Numerical modeling. Journal of Structural Engineering ASCE 1997;123(6):713–20.

[15] Franssen JM, Talamona D, Kruppa J, Cajot LG. Stability of steel columns in case of fire: experimental evaluation. Journal of Structural Engineering, ASCE 1998;124(2):158–63.

[16] Bailey CG, Burgess IW, Plank RJ. The lateral–torsional buckling of unrestrained steel beams in fire. Journal of Constructional Steel Research 1996;36(2):101–19.

[17] Piloto PAG, Vila Real PMM. Lateral torsional buckling of steel I-beams in case of fire — experimental evaluation. In: Proceedings of the first international workshop on structures in fire. 2000. p. 95–105.

[18] Vila Real PMM, Franssen JM. Lateral torsional buckling of steel I-beams in case of fire — numerical modeling. In: Proceedings of the first international workshop on structures in fire. 2000. p. 71–93.

[19] Vila Real PMM, Cazeli R, Simoes da Silva L, Santiago A, Piloto P. The effect of residual stress in the lateral torsional buckling of steel I-beams at elevated temperature. Journal of Constructional Steel Research 2004;60: 783–93.

[20] Vila Real PMM, Lopes N, Simoes da Silva L, Franssen JM. Lateral–torsional buckling of unrestrained steel beams under fire conditions: Improvement of EC3 proposal. Computers & Structures 2004; 82:1737–44.

[21] Timoshenko SP, Gere JM. Theory of elastic stability. 2nd ed. McGraw-Hill Book Company, Inc; 1961.

[22] Lopes N, Simoes da Silva L, Vila Real PMM, Piloto P. New proposals for the design of steel beam–columns in case of fire, including a new approach for the lateral–torsional buckling. Computers & Structures 2004; 82:1463–72.